Correlation-promoted electron-phonon coupling and superconductivity in bulk FeSe

Lan-Lin Du,[1,2] Shiqi Hu,[1] Yang Yang,[1,2] Xuande Bu,[1,2] and Sheng Meng[1,2,3,*]

[1]*Beijing National Laboratory for Condensed Matter Physics and Institute of Physics, Chinese Academy of Sciences, Beijing 100190, People's Republic of China*

[2]*School of Physical Sciences, University of Chinese Academy of Sciences, Beijing 100049, People's Republic of China*

[3]*Songshan Lake Materials Laboratory, Dongguan, Guangdong 523808, People's Republic of China*

(Received 5 August 2025; revised 19 October 2025; accepted 3 November 2025; published 21 November 2025)

Electron-phonon coupling (EPC) plays an important role in FeSe, yet theoretical predictions have struggled to reconcile with experiments on doping- and pressure-dependent superconductivity. Here, we employ dynamical mean-field theory to investigate correlation-corrected EPC in FeSe under carrier doping and pressure. By incorporating correlation-corrected EPC strength and applying the Migdal-Eliashberg formalism for phonon-mediated superconductivity, we predict superconducting transition temperatures T_c that closely match experiments and reproduce the observed doping- and pressure-dependent trends. We further find that the electronic correlation strength, characterized by the bandwidth near the Fermi level, shows an opposite trend to T_c, in contrast to EPC. Our work demonstrates the consistency of the correlation-promoted EPC and T_c over a range of experimental conditions, which suggests that superconductivity in FeSe may originate primarily from correlation-promoted electron-phonon coupling.

DOI: 10.1103/9qx8-7q4x

I. INTRODUCTION

The study of superconductivity has made significant strides over the past several decades, particularly with the discovery of unconventional superconductors, which exhibit superconducting states that cannot be explained by the classical Bardeen-Cooper-Schrieffer (BCS) theory [1]. These materials, including cuprates [2], heavy fermion systems [3], and iron-based superconductors [4], often display unique properties such as non-s-wave pairing symmetries, the coexistence of magnetism and superconductivity, and complex phase diagrams. In unconventional superconductors, the nature of the electron-phonon coupling (EPC) and its impact on the superconducting state remains a topic of intense debate. While electron-electron interactions, such as those arising from strong correlation or spin fluctuations, are believed to dominate in many cases [1–4], an increasing number of experimental studies suggest that EPC plays a crucial role in their superconductivity mechanism [5–10]. It is possible that all these superconductors share a common origin, although it is undeniable that electron correlation-related phenomena, such as experimentally observed quantum criticality [11], strange metal behavior [12], and the theoretically established nonperturbative quantum field theory, continue to pose significant challenges. For example, there is evidence for s-wave pairing symmetry in some copper- and iron-based superconductors [13–15], and the EPC-enhanced superconductivity in specific iron-based superconductors has garnered widespread attention [6–10]. These findings underscore the urgent need to carefully scrutinize the roles of EPC in these systems.

One key argument against EPC as the pairing mechanism in unconventional superconductors is the discrepancy between the first-principles-calculated T_c and the experimentally observed values [16,17]. However, standard density functional theory (DFT), limited by the choice of exchange-correlation functionals, often underestimates the electronic correlation effect in these materials, which in turn leads to an inaccurate estimation of both EPC strength and T_c. Although several promising approaches have been developed to address these limitations, such as density functional perturbation theory combined with Hubbard on-site coulomb interaction U (DFPT + U) [18,19], GW perturbation theory (GWPT) [20,21], and density functional theory plus dynamical mean-field theory (DFT + DMFT) approaches [22,23], the consistency between the existing theoretical analyses and the experimental data is still missing.

Iron selenide (FeSe), as a prominent member of the iron-based superconductors with the simplest crystal structure among them, has a relatively low superconducting transition temperature ($T_c \approx 8$ K). Under high pressures, it exhibits an enhanced superconducting transition temperature, reaching up to 37 K at a pressure around 8 GPa [24]. As the doping level increases, the superconducting T_c of bulk FeSe first decreases to 0, then increases to a maximum of nearly 40 K [25]. This sensitivity to pressure and the doping level is thought to be related to its electronic structure and the stength of electron correlation in the material, but its exact origin has escaped careful scrutiny.

In this work, building upon the methodology established in Ref. [23], we adopt first-principles DMFT plus frozen phonon calculations [22,23,26] to systematically explore the electronic structure and EPC behavior of bulk FeSe. While Ref. [23] has already demonstrated the important role of

*Contact author: smeng@iphy.ac.cn

electron correlations in enhancing EPC in pristine bulk FeSe, our study goes beyond by explicitly examining their evolution under different doping levels and external pressure. The calculated T_c and correlation strength behavior are all consistent with the above mentioned experimental observations. Interestingly, we find that the electronic correlation strength, characterized by the bandwidth near the Fermi level, shows a trend opposite to that of T_c, in contrast to the behavior of EPC. The good agreement between the experimental and our theoretical data suggests that superconductivity in FeSe may primarily originate from EPC, which is largely promoted by the electron correlation effect comparing to the static mean-field results.

II. METHODOLOGY

We employ the QUANTUM ESPRESSO package [27,28] to calculate the phonon dispersion and EPC strength in the framework of density functional perturbation theory. The TRIQS/SOLID_DMFT package [29,30] is used for the DMFT calculations. Norm-conserving pseudopotentials [31] are employed to describe the valence electrons, and the exchange-correlation functionals are treated using the local density approximation (LDA) to ensure better compatibility with DMFT. For FeSe, a *p-d* Hamiltonian with density-density type interactions is applied to describe the electronic correlations, which are solved using the hybridization expansion version of the continuous-time quantum Monte Carlo method [32]. For the analytic continuation of the Green's functions, we use the maximum entropy method as implemented in the TRIQS/MAXENT package [33]. We set the on-site Coulomb interaction $U = 5\,\mathrm{eV}$ and the Hund's coupling $J = 0.8\,\mathrm{eV}$, which are reasonable for bulk FeSe [22,23].

The deformation potential is defined as the band shift caused by unit atomic distortion along the vector direction of a given phonon mode, which is given by [23]

$$D_\nu(n\mathbf{k}) = \left|\left(\epsilon_{n\mathbf{k}}^{\text{original}} + \mu^{\text{original}}\right) - \left(\epsilon_{n\mathbf{k}}^{\text{distorted}} + \mu^{\text{distorted}}\right)\right|, \tag{1}$$

where $\epsilon_{n\mathbf{k}}^{\text{original}}$ and $\epsilon_{n\mathbf{k}}^{\text{distorted}}$ are the electronic energies of the original and distorted configurations with band and momentum indices n and $\mathbf{k}$, respectively. μ^{original} and $\mu^{\text{distorted}}$ are the corresponding chemical potentials. To extract the quasiparticle dispersion from our DMFT calculations, we first performed the analytic continuation of the local self-energy to the real-frequency axis and obtain the Green's function $G_n(\mathbf{k}, \omega)$ using the maximum entropy method, where ω is the Matsubara frequency. The momentum-resolved spectral function in the band representation is then given by

$$A_n(\mathbf{k}, \omega) = -\frac{1}{\pi}\,\mathrm{Im}\,G_n(\mathbf{k}, \omega). \tag{2}$$

For each band at a given momentum $\mathbf{k}$, we identify the quasiparticle energy $\epsilon_{n\mathbf{k}}$ as the frequency ω at which $A_n(\mathbf{k}, \omega)$ reaches its maximum within the energy window of interest.

Since forward scattering (small $\mathbf{q}$) contributes dominantly to the EPC in FeSe [6,8,26,34], the phonon-assisted interband processes ($m \neq n$) on the Fermi surface are forbidden, except at isolated $\mathbf{k}$ points where band degeneracies occur. Consequently, the contribution from interband EPC matrix elements is negligibly small, and the EPC is well described by the intraband components. Therefore, D_ν of the phonon modes at the Γ point defined in Eq. (1) represents the main EPC matrix elements to be considered in the full EPC strength λ. The mode-resolved EPC strength λ_ν is given by [23]

$$\lambda_\nu \approx N_{\text{nest}} \left\langle D_\nu^2(n\mathbf{k})\right\rangle_{\text{FS}} / (\hbar\omega_\nu), \tag{3}$$

where $\langle D_\nu^2(n\mathbf{k})\rangle_{\text{FS}}$ is the average value of $D_\nu(n\mathbf{k})$ squared on the Fermi surface (FS). The ω_ν represents the frequency of the corresponding phonon mode. N_{nest} is the Fermi surface nesting factor, which is approximately proportional to the density of states at the Fermi level N_F in FeSe. From Eq. (3), we can correct the λ_ν obtained from DFT calculations using DMFT as follows:

$$\lambda_\nu^{\text{DMFT}} \approx \frac{N_F^{\text{DMFT}} \left\langle D_\nu^2(n\mathbf{k})\right\rangle_{\text{FS}}^{\text{DMFT}}}{N_F^{\text{DFT}} \left\langle D_\nu^2(n\mathbf{k})\right\rangle_{\text{FS}}^{\text{DFT}}} \lambda_\nu^{\text{DFT}}. \tag{4}$$

The superscripts correspond to the methods used to calculate these quantities. The total EPC strength λ is the sum of λ_ν for each mode at different phonon momentum ($\mathbf{q}$) points. Then, using the McMillan-Allen-Dynes equation [35,36], the superconducting T_c can be evaluated as

$$k_B T_c = \frac{\hbar\omega_{\ln}}{1.2} \exp\left[-\frac{1.04(1+\lambda)}{\lambda - \mu^*(1+0.62\lambda)}\right], \tag{5}$$

where $\omega_{\ln}$ is the logarithmic average of phonon frequencies and μ^* is the screened Coulomb parameter, typically lying in the range of 0.1–0.2 [37,38]. In the present work μ^* is set as 0.12.

III. RESULTS

A. Electronic structure and electron-phonon couplings of bulk FeSe

FeSe crystallizes in a tetragonal PbO-type structure (space group $P4/nmm$), consisting of stacked layers of edge-sharing $FeSe_4$ tetrahedra, with lattice constant $a = b = 3.765\,\text{Å}$ and $c = 5.518\,\text{Å}$, and the height of Se atoms from the Fe plane is $\pm 0.267c$. The calculated spectral function of bulk FeSe from DMFT $A(k, \omega)$ is shown in Fig. 1(a). The renormalization factors for the α, β, and γ bands, modified by DMFT from the DFT values, are 1.8, 3.3, and 2.4, respectively, which are consistent with the previous studies [23,39–41]. Notably, the gap between the electron pocket at the M point below the Fermi surface and the pocket beneath it, which is present in the DFT calculations, closes in the DMFT calculations. The latter is consistent with the experimental result [42,43], thus validating the accuracy of our DMFT calculations.

As the next step, we calculate the phonon properties of bulk FeSe and use them to evaluate the deformation potential and EPC strengths within either the DFT or DMFT framework, employing the frozen phonon approach. Figure 1(b) shows the phonon spectrum and the distribution of the EPC strength, which confirms the property of forward scattering (for more details, see the Appendix). The eigenvector $e_{\nu\mathbf{q},\kappa\alpha}$ of the optical phonon modes at Γ point ($\mathbf{q} = 0$) with $\kappa\alpha$ labeling the Cartesian coordinates of the κth atom are shown in Fig. 1(c). The atomic structural displacement is given as

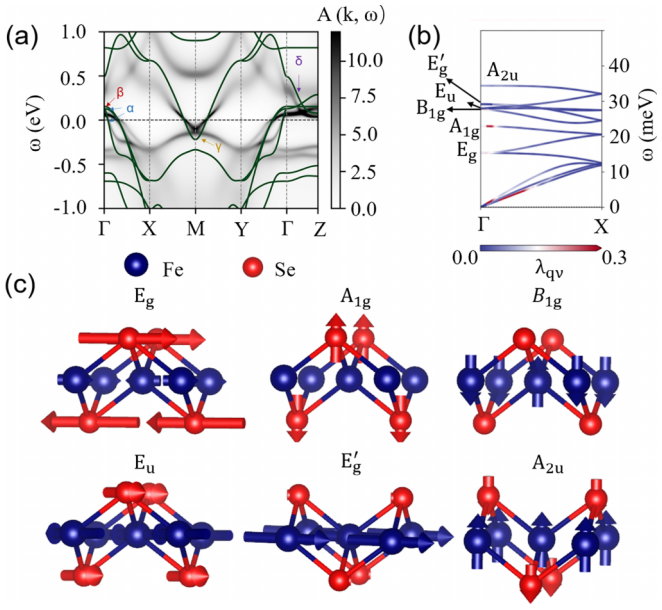

FIG. 1. (a) The DMFT spectral function $A(k, \omega)$ of bulk FeSe. The green solid lines are the band structure from DFT. (b) The phonon spectrum and the distribution of the EPC strength. (c) The eigenvectors of the optical phonon modes at the Γ point.

$\Delta \boldsymbol{l}_{\nu,\kappa\alpha} = \sqrt{\frac{\hbar}{2m_\kappa \omega_\nu}} \boldsymbol{e}_{\nu,\kappa\alpha}$ [38]; m_κ is the atomic mass of the κth atom in the unit cell. The results of the calculated deformation potential and EPC strength are summarized in Table I. The changes in the DMFT-calculated spectral function near the Fermi surface before and after structural stretching along a given phonon mode are shown in Fig. 2.

The deformation potentials averaged over the respective Fermi surface, as calculated by DMFT, are significantly enhanced compared to those obtained from DFT. Consequently, the EPC strength $\lambda_\nu^{\mathrm{DMFT}}$, calculated using Eq. (4), is also notably enhanced compared to $\lambda_\nu^{\mathrm{DFT}}$. Using the Migdal-Eliashberg formalism, we finally obtain $T_c^{\mathrm{DMFT}} = 12$ K, as compared to $T_c^{\mathrm{DFT}} \sim 0$, while the experimental value is about 8 K. Our results in bulk FeSe prove that electron correlation can greatly enhance the EPC strength in FeSe. Next, we will further verify the decisive role of correlation-enhanced EPC on superconductivity under both carrier doping and high pressure conditions.

TABLE I. Phonon energies $\hbar\omega_\nu$ (meV), Fe and Se atomic displacements Δl (Å), deformation potentials D_ν (meV), and EPC strength λ_ν for each optical phonon mode. Values are calculated within DMFT and DFT.

Phonon mode	E_g	A_{1g}	B_{1g}	E_u	E'_g	A_{2u}
$\hbar\omega_\nu$ (meV)	15.4	23.0	27.8	28.0	29.2	34.4
Δl_{Fe} (Å)	0.010	0.000	0.023	0.019	0.022	0.017
Δl_{Se} (Å)	0.029	0.025	0.000	0.013	0.005	0.012
D_ν^{DMFT} (meV)	27.2	21.1	14.9	12.2	8.6	23.8
D_ν^{DFT} (meV)	5.5	16.1	10.8	0.5	10.7	1.2
$\lambda_\nu^{\mathrm{DMFT}}$	2.64	0.81	0.44	0.62	0.71	2.35
$\lambda_\nu^{\mathrm{DFT}}$	0.13	0.155	0.0899	0.0001	0.1877	0.0039

B. Doping level dependence

In alkali-metal potassium-doped FeSe ultrathin films, Ref. [25] gives a phase diagram with two disconnected superconducting phases and a generally wide nonsuperconducting valley in between. That is, in the weakly doped region, T_c decreases with the increase of doping.

We first consider the case of weak doping. To ensure consistency between the phonon-spectrum and DMFT calculations, we introduce carrier doping into the self-consistent process of DFT. We perform the same calculations as in the previous section for bulk FeSe under two weakly doping levels corresponding to 0.07 and 0.10 electrons per Fe atom. Figure 3(a) shows the spectral functions near the Fermi level for these three doping levels, which shift downward as the doping level increases. The variation of T_c as a function of doping level calculated by DMFT is shown as the red line in Fig. 3(b). The blue line is obtained by extracting data from Ref. [25]. In weakly doped region, the calculated T_c from correlation-enhanced EPC decreases with the increase of doping, which agrees well with the experimental results. Meanwhile, the bandwidth near the Fermi surface decreases as the electron doping level increases as shown in Fig. 3(c). In detail, the bandwidth of the electron pocket at the M point becomes significantly narrower with doping, while the bandwidth of the hole pocket at the Γ point remains almost unchanged, which are consistent with the experimental trends [44]. These results indicate that the superconducting T_c is determined by the correlation-enhanced EPC strength, but not directly the strength of electron correlation itself, demonstrating the applicability of correlation-enhanced EPC as the main origin of superconductivity in FeSe under weakly doped conditions.

Experiments on $K_xFe_{2-y}Se_2$ show that the T_c exceeds 30 K [45–48], which falls in the heavily doped region. Due to the self-interaction errors in DFT, the direct carrier doping method is no longer applicable in the heavily doped region. Therefore, we explore the heavily doped situation by calculating the bulk material $K_xFe_{2-y}Se_2$. To simplify the calculation, we choose bulk KFe_2Se_2 and perform the same calculations as in the previous sections. The crystal structure of KFe_2Se_2 can be seen as potassium atoms inserted between the layers of bulk FeSe, as shown in Fig. 4(a). First, we focus on the characteristics of the DMFT spectral function, as shown in Fig. 4(b). A clear electron pocket appears at the Γ point, consistent with experimental measurements [49]. The discrepancy between the number of electron pockets observed at the Γ point in the experiment (two, as reported in Ref. [49]) and in our calculations (one) can be attributed to the inequivalence of different Fe atoms in the experiment, which leads to a breaking of degeneracy. Furthermore, we emphasize that in DMFT calculations, the electronic gap opens between the electron pocket at the M point below the Fermi surface and the pocket below it, which was experimentally observed in potassium-doped FeSe [50].

To evaluate the critical temperature T_c of superconductivity, we use the EPC calculated from the DMFT plus frozen

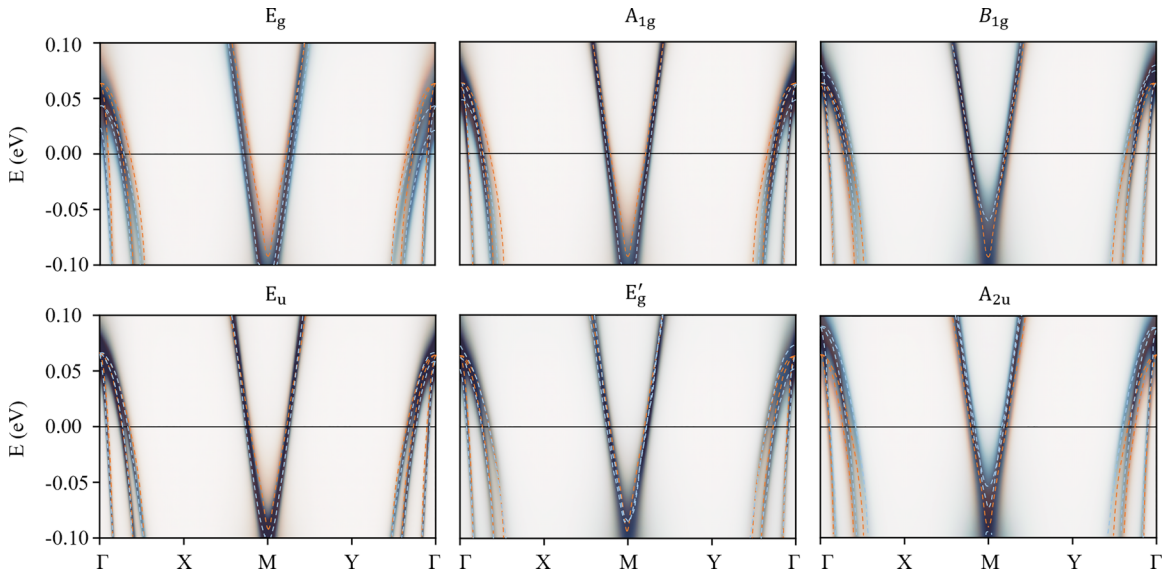

FIG. 2. Spectral functions of bulk FeSe without (orange) and with (blue) a given phonon excitation within the DFT + DMFT for all the optical phonon modes. The Fermi surface is corrected to be consistent with the unperturbed state. The dotted lines are for easier viewing.

phonon approach. The T_c of 18.5 K is obtained for KFe_2Se_2, which is higher than the 12.0 K obtained for bulk FeSe. In contrast, the T_c from static DFT calculations is close to 0 K, similar to the value for bulk FeSe. It is worth noting that our calculated T_c is smaller than the experimental result of >30 K of $K_{0.68}Fe_{1.79}Se_2$ [49], which may be due to the different stoichiometric ratios in experiment. Our theoretical results are qualitatively consistent with the experimental results, which demonstrate the applicability of correlation-enhanced EPC as the main origin of superconductivity in FeSe under heavily doped conditions.

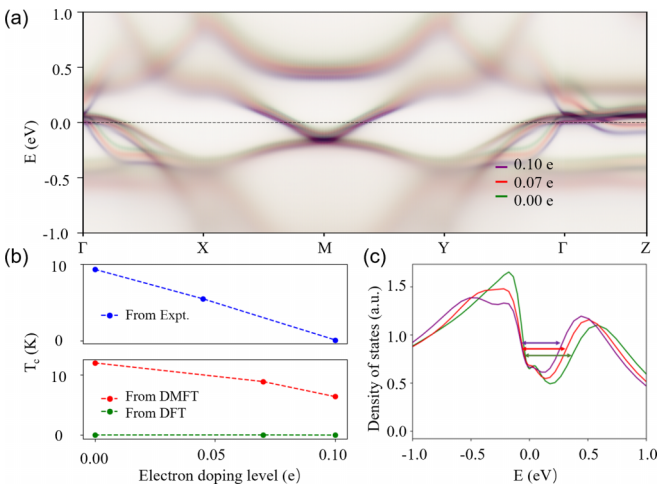

FIG. 3. (a) The spectral functions near the Fermi level for the three doping levels. (b) Red (green) line: The specific variation of the T_c calculated by DMFT plus frozen phonon method (calculated by LDA approximation) as a function of doping level. Blue line: experimental data from Ref. [25]. For a direct comparison, the doping level is rescaled by 5 times for experiments. (c) The corresponding density of states near the Fermi surface for the three doping levels. The changes in the length of the arrows reflect the changes in bandwidth for the three doping levels.

C. Correlation-enhanced superconductivity under pressure

High pressure is another typical way for tuning quantum materials. Specifically, in FeSe, applying pressure causes the superconducting T_c to gradually increase from 0 to about 37 K within the pressure range of 0–8 GPa, and then decrease again with higher pressures, accompanied by a structural phase transition [24,51]. This suggests that pressurizing FeSe in its original configuration enhances T_c, while the configuration under high pressure is detrimental to superconductivity and suppresses T_c.

To explore the behavior of the EPC in FeSe under pressure, we calculated the DMFT-corrected EPC strength and the corresponding superconducting T_c using the experimental lattice parameters a and c from Ref. [24]. Figure 5(a) shows the spectral functions of DMFT under three different pressures. As pressure increases, the bandwidth of the energy bands near the Fermi surface broadens, indicating that the electronic correlation strength weakens with increasing pressure in bulk

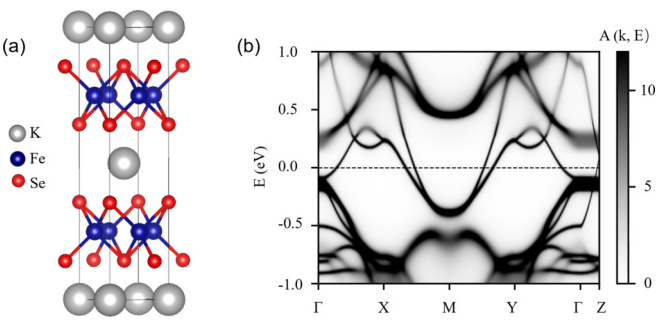

FIG. 4. (a) The atomic structure of bulk KFe_2Se_2. (b) The DMFT spectral function of bulk KFe_2Se_2.

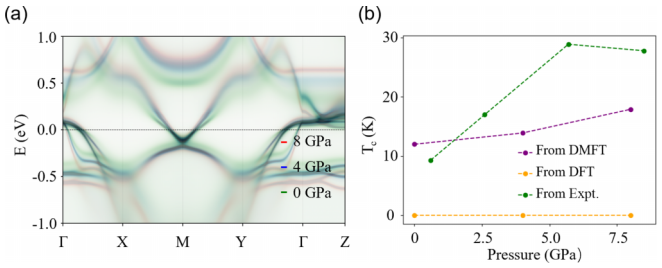

FIG. 5. (a) The spectral functions near the Fermi level for the three pressures. (b) Pressure dependence of the superconducting T_c from DMFT and DFT calculations and experiment. These experimental data are cited from Ref. [24].

FeSe. The strength of the electronic correlation effect is opposite to the behavior of T_c with pressure, indicating that the electronic correlation effect does not directly determine superconductivity.

For clarity, we plot both experimental and theoretical datas for T_c as a function of pressure in Fig. 5(b). The trend of T_c increasing with pressure is consistent in the DMFT and experimental results, while the T_c's calculated by DFT are all close to 0 under the three pressures. The consistency between experimental and calculated results from the DMFT plus frozen phonon approach demonstrate the applicability of correlation-enhanced EPC as the main origin of superconductivity in FeSe under pressure.

IV. DISCUSSION AND CONCLUSION

We first point out that the quantitative difference between the present work and the experimental values may come from the limitations of the computational methods, which do not affect our qualitative conclusions. Since we use one-shot DFT + DMFT calculations, which usually overestimate the electronic correlation strength, the $\lambda_\nu^{\mathrm{DMFT}}$ we calculate could be also overestimated. We choose the size of q mesh in the Migdal-Eliashberg formalism as $4 \times 4 \times 1$ to obtain a T_c close to the experimental value in the calculations of original bulk FeSe, and keep it consistent in the calculations of other cases. It should be noted that a direct evaluation of $\lambda_\nu^{\mathrm{DMFT}}$ through the frozen phonon method would require an unfeasibly large number of correlated calculations with many small atomic displacements to reach numerically converged results. Therefore, following the established approach of Ref. [23], the scaling method adopted in Eq. (4) provides a practical and physically justified means to capture the dominant effects of electronic correlation on EPC. We note that Fig. 3(b) primarily illustrates the variation of T_c in the weak-doping regime, where our calculations reproduce the experimental trend qualitatively. The fact that T_c in Fig. 3(b) does not reach zero within the plotted doping range reflects a limitation of the present computational protocol rather than a physical inconsistency: extending the DMFT-based treatment employed here to the substantially larger carrier dopings required to observe vanishing T_c is numerically challenging due to the increasing self-interaction errors. In addition, we note that the quasilinear dependence of T_c on λ for the forward scattering derived in Ref. [34] is not directly applicable in our case, as the correlation-enhanced λ obtained here lies beyond the weak-coupling regime assumed in that formulation. Another point to note is that in our calculations the E_g and A_{2u} phonon modes show stronger EPC strength than the A_{1g} mode, while the latter has been shown to couple more effectively with electrons [26]. This observation warrants further experimental verification.

Our results highlight the essential role of electronic correlations in enhancing the effective electron-phonon coupling in bulk FeSe. In this context, it is worth comparing our approach with recent developments that combine DMFT with first-principles EPC methods. Reference [52] applied DMFT corrections to the electronic structure entering DFPT, while Ref. [53] incorporated DMFT-derived Green's functions to evaluate the electron-phonon self-energy. More recently, Ref. [54] introduced the DMFT self-energy from finite-displacement phonon perturbation into the Kohn-Sham potential of DFPT calculations, enabling the computation of EPC matrix elements in a way that is conceptually consistent with our frozen-phonon-based method. Similar correlated frameworks have also been employed to investigate FeSe under pressure, yielding results consistent with the general trend observed in our study [55]. Overall, these developments reinforce the growing consensus that electronic correlations play a crucial role in shaping EPC-related phenomena, including superconductivity and transport behavior.

The dramatic enhancement of EPC strength obtained from DMFT calculations compared to static standard DFT calculations inspires us to rethink the EPC properties in correlated materials, and further ponder the origin of unconventional superconductivity. Our results of the bandwidths near the Fermi surface in weakly doped and pressured materials indicate that the superconducting T_c is not directly determined by the correlation strength itself, but the electron-correlation-enhanced EPC strength. In fact, there are already many experimental signatures that unconventional superconductivity might originate from EPC and may have the s-wave pairing symmetry [6–10,13–15,56,57]. The consistency between our calculated T_c from correlation-promoted EPC and the experimentally measured values under various conditions of carrier doping and pressurization provides strong evidence that phonon-mediated electron pairing may be the main origin of superconductivity in unconventional FeSe, while electronic correlation also plays a nontrivial role. At the same time, we note that substantial experimental evidence points to the importance of spin fluctuations, including the spin resonance and gap anisotropy [58–61]. These features suggest that spin fluctuations may cooperate with, or compete against, EPC in shaping the pairing symmetry and superconducting properties of FeSe. We further note that a number of theoretical studies have analyzed superconductivity in FeSe under doping and pressure within spin-fluctuation frameworks [62–66], and these works provide complementary perspectives to our correlation-promoted EPC picture. These spin-fluctuation results do not invalidate the importance of EPC found in our work; rather, they point to a multicomponent pairing landscape in FeSe where spin fluctuations and correlation-enhanced EPC can cooperate or compete depending on doping, pressure, and details of the electronic structure. A complete microscopic description of T_c across the phase diagram therefore requires accounting for

the interplay between electron correlations, EPC, and spin fluctuations.

Finally, we note that isotope effects have been reported in FeSe-related systems. For example, in bulk FeSe, an Fe-isotope substitution experiment [67] reported a nonzero shift of T_c, although part of the observed shift has been attributed to concurrent small structural changes and therefore the intrinsic phonon-mediated isotope exponent requires careful separation of structural and electronic contributions. Also, in FeSe/$STiO_3$ heterostructures, an oxygen-isotope experiment [10] provided strong evidence that substrate oxygen phonons affect the FeSe electrons and T_c. Within our framework, the correlation-enhanced EPC implies that a finite isotope response is expected in principle, although its magnitude may be strongly influenced by the dominant phonon modes and by competing spin-fluctuation channels.

In conclusion, we have employed DMFT in combination with the Migdal-Eliashberg formalism to investigate phonon-mediated superconductivity of FeSe. The electron-correlation-corrected EPC strength and superconducting T_c under different doping and pressure conditions have been calculated. Our results, obtained under various conditions, are qualitatively and even quantitatively consistent with experimental observations. The opposite trend between electronic correlation strength and T_c, compared to the parallel behavior of EPC and T_c, provides further insight into the intertwined roles of electronic correlation and EPC in FeSe. These findings highlight the critical role of EPC in FeSe superconductivity and provide theoretical support for the recent experimental discovery of s-wave pairing symmetry and EPC-driven superconductivity in FeSe. Furthermore, the significant enhancement of EPC by the electronic correlation effect encourages us to reconsider the role of EPC in unconventional superconductors, where electrons are typically thought to be paired by unconventional mechanisms such as correlation-mediated spin fluctuations and where electron-phonon couplings are usually thought to be irrelevant to superconductivity.

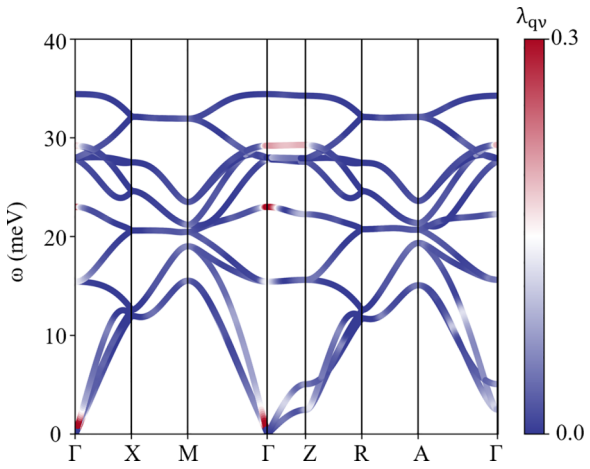

FIG. 6. Phonon dispersions of bulk FeSe, with the EPC strength (λ_{qv}) (represented in color bar) indicating the dominant contributions from phonons around the Γ point (small $|\mathbf{q}|$) to EPC.

ACKNOWLEDGMENTS

This work is supported by the National Natural Science Foundation of China (Grants No. 12025407 and No. 12450401), the Chinese Academy of Sciences (Grants No. YSBR-047 and No. XDB33030100), and the Ministry of Science and Technology (Grant No. 2021YFA1400201).

L.-L.D. and S.H. contributed equally to this work.

DATA AVAILABILITY

The data that support the findings of this article are not publicly available upon publication because it is not technically feasible and/or the cost of preparing, depositing, and hosting the data would be prohibitive within the terms of this research project. The data are available from the authors upon reasonable request.

APPENDIX

To further confirm the forward scattering in FeSe, in Fig. 6 we show the EPC strength of all the phonons along the high-symmetry $\mathbf{q}$ path. It clearly demonstrates that the coupling strength is indeed peaked at small $|\mathbf{q}|$, consistent with the forward-scattering character.

[1] G. R. Stewart, Unconventional superconductivity, Adv. Phys. **66**, 75 (2017).

[2] A. Damascelli, Z. Hussain, and Z.-X. Shen, Angle-resolved photoemission studies of the cuprate superconductors, Rev. Mod. Phys. **75**, 473 (2003).

[3] B. White, J. Thompson, and M. Maple, Unconventional superconductivity in heavy-fermion compounds, Phys. C (Amsterdam, Neth.) **514**, 246 (2015).

[4] R. M. Fernandes, A. I. Coldea, H. Ding, I. R. Fisher, P. J. Hirschfeld, and G. Kotliar, Iron pnictides and chalcogenides: A new paradigm for superconductivity, Nature (London) **601**, 35 (2022).

[5] A. Lanzara, P. V. Bogdanov, X. J. Zhou, S. A. Kellar, D. L. Feng, E. D. Lu, T. Yoshida, H. Eisaki, A. Fujimori, K. Kishio, J.-I. Shimoyama, T. Noda, S. Uchida, Z. Hussain, and Z.-X. Shen, Evidence for ubiquitous strong electron–phonon coupling in high-temperature superconductors, Nature (London) **412**, 510 (2001).

[6] J. J. Lee, F. T. Schmitt, R. G. Moore, S. Johnston, Y.-T. Cui, W. Li, M. Yi, Z. K. Liu, M. Hashimoto, Y. Zhang, D. H. Lu, T. P. Devereaux, D.-H. Lee, and Z.-X. Shen, Interfacial mode coupling as the origin of the enhancement of T_c in FeSe films on $SrTiO_3$, Nature (London) **515**, 245 (2014).

[7] C. Tang, C. Liu, G. Zhou, F. Li, H. Ding, Z. Li, D. Zhang, Z. Li, C. Song, S. Ji, K. He, L. Wang, X. Ma, and Q.-K. Xue, Interface-enhanced electron-phonon coupling and high-temperature superconductivity in potassium-coated ultrathin FeSe films on $SrTiO_3$, Phys. Rev. B **93**, 020507(R) (2016).

[8] S. N. Rebec, T. Jia, C. Zhang, M. Hashimoto, D.-H. Lu, R. G. Moore, and Z.-X. Shen, Coexistence of replica bands and superconductivity in FeSe monolayer films, Phys. Rev. Lett. **118**, 067002 (2017).

[9] S. Zhang, T. Wei, J. Guan, Q. Zhu, W. Qin, W. Wang, J. Zhang, E. W. Plummer, X. Zhu, Z. Zhang, and J. Guo, Enhanced superconducting state in $FeSe/SrTiO_3$ by a dynamic interfacial polaron mechanism, Phys. Rev. Lett. **122**, 066802 (2019).

[10] Q. Song, T. L. Yu, X. Lou, B. P. Xie, H. C. Xu, C. H. P. Wen, Q. Yao, S. Y. Zhang, X. T. Zhu, J. D. Guo, R. Peng, and D. L. Feng, Evidence of cooperative effect on the enhanced superconducting transition temperature at the $FeSe/SrTiO_3$ interface, Nat. Commun. **10**, 758 (2019).

[11] S. Kirchner, S. Paschen, Q. Chen, S. Wirth, D. Feng, J. D. Thompson, and Q. Si, *Colloquium*: Heavy-electron quantum criticality and single-particle spectroscopy, Rev. Mod. Phys. **92**, 011002 (2020).

[12] P. W. Phillips, N. E. Hussey, and P. Abbamonte, Stranger than metals, Science **377**, eabh4273 (2022).

[13] Y. Zhong, Y. Wang, S. Han, Y.-F. Lv, W.-L. Wang, D. Zhang, H. Ding, Y.-M. Zhang, L. Wang, K. He, R. Zhong, J. A. Schneeloch, G.-D. Gu, C.-L. Song, X.-C. Ma, and Q.-K. Xue, Nodeless pairing in superconducting copper-oxide monolayer films on $Bi_2Sr_2CaCu_2O_{8+\delta}$, Sci. Bull. **61**, 1239 (2016).

[14] Y. Zhu, M. Liao, Q. Zhang, H.-Y. Xie, F. Meng, Y. Liu, Z. Bai, S. Ji, J. Zhang, K. Jiang, R. Zhong, J. Schneeloch, G. Gu, L. Gu, X. Ma, D. Zhang, and Q.-K. Xue, Presence of *s*-wave pairing in Josephson junctions made of twisted ultrathin $Bi_2Sr_2CaCu_2O_{8+x}$ flakes, Phys. Rev. X **11**, 031011 (2021).

[15] Q. Fan, W. H. Zhang, X. Liu, Y. J. Yan, M. Q. Ren, R. Peng, H. C. Xu, B. P. Xie, J. P. Hu, T. Zhang, and D. L. Feng, Plain *s*-wave superconductivity in single-layer FeSe on $SrTiO_3$ probed by scanning tunnelling microscopy, Nat. Phys. **11**, 946 (2015).

[16] A. Subedi, L. Zhang, D. J. Singh, and M. H. Du, Density functional study of FeS, FeSe, and FeTe: Electronic structure, magnetism, phonons, and superconductivity, Phys. Rev. B **78**, 134514 (2008).

[17] R. Heid, K.-P. Bohnen, R. Zeyher, and D. Manske, Momentum dependence of the electron-phonon coupling and self-energy effects in superconducting $YBa_2Cu_3O_7$ within the local density approximation, Phys. Rev. Lett. **100**, 137001 (2008).

[18] A. Floris, I. Timrov, B. Himmetoglu, N. Marzari, S. de Gironcoli, and M. Cococcioni, Hubbard-corrected density functional perturbation theory with ultrasoft pseudopotentials, Phys. Rev. B **101**, 064305 (2020).

[19] B. K. Chang, I. Timrov, J. Park, J.-J. Zhou, N. Marzari, and M. Bernardi, First-principles electron-phonon interactions and polarons in the parent cuprate La_2CuO_4, Phys. Rev. Res. **7**, L012073 (2025).

[20] Z. Li, G. Antonius, M. Wu, F. H. da Jornada, and S. G. Louie, Electron-phonon coupling from *ab initio* linear-response theory within the *GW* method: Correlation-enhanced interactions and superconductivity in $Ba_{1-x}K_xBiO_3$, Phys. Rev. Lett. **122**, 186402 (2019).

[21] Z. Li and S. G. Louie, Two-gap superconductivity and the decisive role of rare-earth *d* electrons in infinite-layer nickelates, Phys. Rev. Lett. **133**, 126401 (2024).

[22] S. Mandal, R. E. Cohen, and K. Haule, Strong pressure-dependent electron-phonon coupling in FeSe, Phys. Rev. B **89**, 220502(R) (2014).

[23] W. Ding, Y. Wang, T. Wei, J. Gao, P. Cui, and Z. Zhang, Correlation-enhanced electron-phonon coupling for accurate evaluation of the superconducting transition temperature in bulk FeSe, Sci. China: Phys. Mech. Astron. **65**, 267412 (2022).

[24] S. Margadonna, Y. Takabayashi, Y. Ohishi, Y. Mizuguchi, Y. Takano, T. Kagayama, T. Nakagawa, M. Takata, and K. Prassides, Pressure evolution of the low-temperature crystal structure and bonding of the superconductor FeSe ($T_c = 37$ K), Phys. Rev. B **80**, 064506 (2009).

[25] C.-L. Song, H.-M. Zhang, Y. Zhong, X.-P. Hu, S.-H. Ji, L. Wang, K. He, X.-C. Ma, and Q.-K. Xue, Observation of double-dome superconductivity in potassium-doped FeSe thin films, Phys. Rev. Lett. **116**, 157001 (2016).

[26] S. Gerber, S.-L. Yang, D. Zhu, H. Soifer, J. A. Sobota, S. Rebec, J. J. Lee, T. Jia, B. Moritz, C. Jia, A. Gauthier, Y. Li, D. Leuenberger, Y. Zhang, L. Chaix, W. Li, H. Jang, J.-S. Lee, M. Yi, G. L. Dakovski *et al.*, Femtosecond electron-phonon lock-in by photoemission and x-ray free-electron laser, Science **357**, 71 (2017).

[27] P. Giannozzi, S. Baroni, N. Bonini, M. Calandra, R. Car, C. Cavazzoni, D. Ceresoli, G. L. Chiarotti, M. Cococcioni, I. Dabo, A. D. Corso, S. de Gironcoli, S. Fabris, G. Fratesi, R. Gebauer, U. Gerstmann, C. Gougoussis, A. Kokalj, M. Lazzeri, L. Martin-Samos *et al.*, QUANTUM ESPRESSO: A modular and open-source software project for quantum simulations of materials, J. Phys.: Condens. Matter **21**, 395502 (2009).

[28] P. Giannozzi, O. Andreussi, T. Brumme, O. Bunau, M. B. Nardelli, M. Calandra, R. Car, C. Cavazzoni, D. Ceresoli, M. Cococcioni, N. Colonna, I. Carnimeo, A. Dal Corso, S. de Gironcoli, P. Delugas, R. A. DiStasio Jr., A. Ferretti, A. Floris, G. Fratesi, G. Fugallo *et al.*, Advanced capabilities for materials modelling with QUANTUM ESPRESSO, J. Phys.: Condens. Matter **29**, 465901 (2017).

[29] O. Parcollet, M. Ferrero, T. Ayral, H. Hafermann, I. Krivenko, L. Messio, and P. Seth, TRIQS: A toolbox for research on interacting quantum systems, Comput. Phys. Commun. **196**, 398 (2015).

[30] M. E. Merkel, A. Carta, S. Beck, and A. Hampel, Solid_dmft: Gray-boxing DFT+DMFT materials simulations with TRIQS, J. Open Source Software **7**, 4623 (2022).

[31] M. van Setten, M. Giantomassi, E. Bousquet, M. Verstraete, D. Hamann, X. Gonze, and G.-M. Rignanese, The PSEUDODOJO: Training and grading a 85 element optimized norm-conserving pseudopotential table, Comput. Phys. Commun. **226**, 39 (2018).

[32] P. Seth, I. Krivenko, M. Ferrero, and O. Parcollet, TRIQS/CTHYB: A continuous-time quantum Monte Carlo hybridisation expansion solver for quantum impurity problems, Comput. Phys. Commun. **200**, 274 (2016).

[33] G. J. Kraberger, R. Triebl, M. Zingl, and M. Aichhorn, Maximum entropy formalism for the analytic continuation of matrix-valued Green's functions, Phys. Rev. B **96**, 155128 (2017).

[34] L. Rademaker, Y. Wang, T. Berlijn, and S. Johnston, Enhanced superconductivity due to forward scattering in FeSe thin films on $SrTiO_3$ substrates, New J. Phys. **18**, 022001 (2016).

[35] W. L. McMillan, Transition temperature of strong-coupled superconductors, Phys. Rev. **167**, 331 (1968).

[36] P. B. Allen and R. C. Dynes, Transition temperature of strong-coupled superconductors reanalyzed, Phys. Rev. B **12**, 905 (1975).

[37] K.-H. Lee, K. J. Chang, and M. L. Cohen, First-principles calculations of the Coulomb pseudopotential μ^*: Application to Al, Phys. Rev. B **52**, 1425 (1995).

[38] F. Giustino, Electron-phonon interactions from first principles, Rev. Mod. Phys. **89**, 015003 (2017).

[39] M. Aichhorn, S. Biermann, T. Miyake, A. Georges, and M. Imada, Theoretical evidence for strong correlations and incoherent metallic state in FeSe, Phys. Rev. B **82**, 064504 (2010).

[40] J. Maletz, V. B. Zabolotnyy, D. V. Evtushinsky, S. Thirupathaiah, A. U. B. Wolter, L. Harnagea, A. N. Yaresko, A. N. Vasiliev, D. A. Chareev, A. E. Böhmer, F. Hardy, T. Wolf, C. Meingast, E. D. L. Rienks, B. Büchner, and S. V. Borisenko, Unusual band renormalization in the simplest iron-based superconductor $FeSe_{1-x}$, Phys. Rev. B **89**, 220506(R) (2014).

[41] M. D. Watson, S. Backes, A. A. Haghighirad, M. Hoesch, T. K. Kim, A. I. Coldea, and R. Valentí, Formation of Hubbard-like bands as a fingerprint of strong electron-electron interactions in FeSe, Phys. Rev. B **95**, 081106(R) (2017).

[42] M. D. Watson, T. K. Kim, A. A. Haghighirad, N. R. Davies, A. McCollam, A. Narayanan, S. F. Blake, Y. L. Chen, S. Ghannadzadeh, A. J. Schofield, M. Hoesch, C. Meingast, T. Wolf, and A. I. Coldea, Emergence of the nematic electronic state in FeSe, Phys. Rev. B **91**, 155106 (2015).

[43] T. Shimojima, Y. Suzuki, T. Sonobe, A. Nakamura, M. Sakano, J. Omachi, K. Yoshioka, M. Kuwata-Gonokami, K. Ono, H. Kumigashira, A. E. Böhmer, F. Hardy, T. Wolf, C. Meingast, H. v. Löhneysen, H. Ikeda, and K. Ishizaka, Lifting of *xz*/*yz* orbital degeneracy at the structural transition in detwinned FeSe, Phys. Rev. B **90**, 121111(R) (2014).

[44] C. H. P. Wen, H. C. Xu, C. Chen, Z. C. Huang, X. Lou, Y. J. Pu, Q. Song, B. P. Xie, M. Abdel-Hafiez, D. A. Chareev, A. N. Vasiliev, R. Peng, and D. L. Feng, Anomalous correlation effects and unique phase diagram of electron-doped FeSe revealed by photoemission spectroscopy, Nat. Commun. **7**, 10840 (2016).

[45] J. Guo, S. Jin, G. Wang, S. Wang, K. Zhu, T. Zhou, M. He, and X. Chen, Superconductivity in the iron selenide $K_xFe_2Se_2 (0 \leqslant x \leqslant 1.0)$, Phys. Rev. B **82**, 180520(R) (2010).

[46] Y. Mizuguchi, H. Takeya, Y. Kawasaki, T. Ozaki, S. Tsuda, T. Yamaguchi, and Y. Takano, Transport properties of the new Fe-based superconductor $K_xFe_2Se_2$ ($T_c = 33$ K), Appl. Phys. Lett. **98**, 042511 (2011).

[47] M.-H. Fang, H.-D. Wang, C.-H. Dong, Z.-J. Li, C.-M. Feng, J. Chen, and H. Q. Yuan, Fe-based superconductivity with T_c=31 K bordering an antiferromagnetic insulator in (Tl, K)Fe_xSe_2, EPL **94**, 27009 (2011).

[48] D. M. Wang, J. B. He, T.-L. Xia, and G. F. Chen, Effect of varying iron content on the transport properties of the potassium-intercalated iron selenide $K_xFe_{2-y}Se_2$, Phys. Rev. B **83**, 132502 (2011).

[49] L. Zhao, D. Mou, S. Liu, X. Jia, J. He, Y. Peng, L. Yu, X. Liu, G. Liu, S. He, X. Dong, J. Zhang, J. B. He, D. M. Wang, G. F. Chen, J. G. Guo, X. L. Chen, X. Wang, Q. Peng, Z. Wang *et al.*, Common Fermi-surface topology and nodeless superconducting gap of $K_{0.68}Fe_{1.79}Se_2$ and $(Tl_{0.45}K_{0.34})Fe_{1.84}Se_2$ superconductors revealed via angle-resolved photoemission, Phys. Rev. B **83**, 140508(R) (2011).

[50] Z. R. Ye, C. F. Zhang, H. L. Ning, W. Li, L. Chen, T. Jia, M. Hashimoto, D. H. Lu, Z. X. Shen, and Y. Zhang, Simultaneous emergence of superconductivity, inter-pocket scattering and nematic fluctuation in potassium-coated FeSe superconductor, arXiv:1512.02526.

[51] S. Medvedev, T. M. McQueen, I. A. Troyan, T. Palasyuk, M. I. Eremets, R. J. Cava, S. Naghavi, F. Casper, V. Ksenofontov, G. Wortmann, and C. Felser, Electronic and magnetic phase diagram of β-$Fe_{1.01}Se$ with superconductivity at 36.7 K under pressure, Nat. Mater. **8**, 630 (2009).

[52] Y. Wei, E. Chachkarova, E. Plekhanov, N. Bonini, and C. Weber, Exploring the effect of the number of hydrogen atoms on the properties of lanthanide hydrides by DMFT, Appl. Sci. **12**, 3498 (2022).

[53] D. J. Abramovitch, J.-J. Zhou, J. Mravlje, A. Georges, and M. Bernardi, Combining electron-phonon and dynamical mean-field theory calculations of correlated materials: Transport in the correlated metal Sr_2RuO_4, Phys. Rev. Mater. **7**, 093801 (2023).

[54] D. J. Abramovitch, J. Coulter, S. Beck, and A. Millis, Electron-phonon coupling in correlated metals: A dynamical mean-field theory study, Phys. Rev. B **112**, 075113 (2025).

[55] Z. Ding, J. Gao, W. Qin, Y. Ma, P. Cui, and Z. Zhang, Multidomed superconductivity and tunable orbital-selective pairing in pressurized FeSe with correlation enhanced electron-phonon coupling, Phys. Rev. B **111**, L220501 (2025).

[56] J.-Q. Fan, X.-Q. Yu, F.-J. Cheng, H. Wang, R. Wang, X. Ma, X.-P. Hu, D. Zhang, X.-C. Ma, Q.-K. Xue, and C.-L. Song, Direct observation of nodeless superconductivity and phonon modes in electron-doped copper oxide $Sr_{1-x}Nd_xCuO_2$, Natl. Sci. Rev. **9**, nwab225 (2022).

[57] Y. Peng, L. Martinelli, Q. Li, M. Rossi, M. Mitrano, R. Arpaia, M. M. Sala, Q. Gao, X. Guo, G. M. De Luca, A. Walters, A. Nag, A. Barbour, G. Gu, J. Pelliciari, N. B. Brookes, P. Abbamonte, M. Salluzzo, X. Zhou, K.-J. Zhou *et al.*, Doping dependence of the electron-phonon coupling in two families of bilayer superconducting cuprates, Phys. Rev. B **105**, 115105 (2022).

[58] Q. Wang, Y. Shen, B. Pan, Y. Hao, M. Ma, F. Zhou, P. Steffens, K. Schmalzl, T. R. Forrest, M. Abdel-Hafiez, X. Chen, D. A. Chareev, A. N. Vasiliev, P. Bourges, Y. Sidis, H. Cao, and J. Zhao, Strong interplay between stripe spin fluctuations, nematicity and superconductivity in FeSe, Nat. Mater. **15**, 159 (2016).

[59] M. Ma, P. Bourges, Y. Sidis, Y. Xu, S. Li, B. Hu, J. Li, F. Wang, and Y. Li, Prominent role of spin-orbit coupling in FeSe revealed by inelastic neutron scattering, Phys. Rev. X **7**, 021025 (2017).

[60] Y. Zhang, J. J. Lee, R. G. Moore, W. Li, M. Yi, M. Hashimoto, D. H. Lu, T. P. Devereaux, D.-H. Lee, and Z.-X. Shen, Superconducting gap anisotropy in monolayer FeSe thin film, Phys. Rev. Lett. **117**, 117001 (2016).

[61] C.-L. Song, Y.-L. Wang, P. Cheng, Y.-P. Jiang, W. Li, T. Zhang, Z. Li, K. He, L. Wang, J.-F. Jia, H.-H. Hung, C. Wu, X. Ma, X. Chen, and Q.-K. Xue, Direct observation of nodes and twofold symmetry in FeSe superconductor, Science **332**, 1410 (2011).

[62] J. P. Sun, G. Z. Ye, P. Shahi, J.-Q. Yan, K. Matsuura, H. Kontani, G. M. Zhang, Q. Zhou, B. C. Sales, T. Shibauchi, Y. Uwatoko, D. J. Singh, and J.-G. Cheng, High-T_c superconductivity in FeSe at high pressure: Dominant hole carriers and enhanced spin fluctuations, Phys. Rev. Lett. **118**, 147004 (2017).

[63] A. Linscheid, S. Maiti, Y. Wang, S. Johnston, and P. J. Hirschfeld, High T_c via spin fluctuations from incipient bands: Application to monolayers and intercalates of FeSe, Phys. Rev. Lett. **117**, 077003 (2016).

[64] L. Benfatto, B. Valenzuela, and L. Fanfarillo, Nematic pairing from orbital-selective spin fluctuations in FeSe, npj Quantum Mater. **3**, 56 (2018).

[65] Y. Yamakawa, S. Onari, and H. Kontani, Doping effects on electronic states in electron-doped FeSe: Impact of self-energy and vertex corrections, Phys. Rev. B **102**, 081108(R) (2020).

[66] S. Acharya, M. I. Katsnelson, and M. van Schilfgaarde, Vertex dominated superconductivity in intercalated FeSe, npj Quantum Mater. **8**, 24 (2023).

[67] R. Khasanov, M. Bendele, K. Conder, H. Keller, E. Pomjakushina, and V. Pomjakushin, Iron isotope effect on the superconducting transition temperature and the crystal structure of $FeSe_{1-x}$, New J. Phys. **12**, 073024 (2010).